A&A 472, 299–307 (2007)
DOI: 10.1051/0004-6361:20077083
© ESO 2007

Astronomy & Astrophysics

Outflow velocity of the O^{+5} ions in polar coronal holes out to 5 $R_\odot$

D. Telloni[1], E. Antonucci[1], and M. A. Dodero[2]

[1] Istituto Nazionale di Astrofisica (INAF), Osservatorio Astronomico di Torino, Strada Osservatorio 20, 10025 Pino Torinese, Italy
e-mail: telloni@to.infn.it
[2] University of Torino, via P. Giuria 1, 10125 Torino, Italy

Received 11 January 2007 / Accepted 21 June 2007

ABSTRACT

The purpose of the paper is to extend the measurement of the kinetic temperature and outflow velocity of the oxygen ions in the outer corona above polar holes out to 5 $R_\odot$. An analytical model of the solar corona at the minimum of activity has been employed in order to synthesize the spectral line profiles to be fitted with the data: the kinetic temperature of the O^{+5} ions on the plane of the sky is derived from the width of the O VI 1031.9 Å line by applying the χ^2 minimization. The oxygen temperature peaks at about 2.9 $R_\odot$, reaching a value of 1.5×10^8 K, and further out it is somehow flattening. The outflow velocity of the oxygen component of the fast solar wind, derived from the intensity ratio of the Doppler dimmed O VI doublet, increases outward to reach 550–760 km s^{-1} at 5 $R_\odot$. The upper and lower limits of the outflow speed are due to the fact that its measurement depends on the velocity distribution of the oxygen ions which cannot be directly measured along the radial direction, but only along the line of sight. Hence the uncertainty is related to the temperature anisotropy assumed in the analysis. For this reason in this paper the measurement of the temperature anisotropy, found beyond 2 $R_\odot$ according to the previous literature on UVCS results, has been as well extended at higher altitudes, and it is found that above 3.7 $R_\odot$ anisotropy can still exist but not necessarily. The observations of the extended corona analyzed in this paper are performed with the Ultraviolet Coronagraph Spectrometer on board the Solar Heliospheric Observatory, during the solar minimum activity period 1996–1997.

Key words. Sun: corona – Sun: UV radiation – Sun: solar wind

1. Introduction

The Ultraviolet Coronagraph Spectrometer (UVCS) on board the Solar Heliospheric Observatory (SOHO) (Kohl et al. 1995) allows to investigate the source and acceleration region of the fast wind and to derive its outflow velocity.

The first observations of UVCS, above the polar regions during the minimum of activity, have revealed that these regions are characterized by unexpected broad profiles of the O VI 1031.9, 1037.6 Å lines. In addition these measurements have allowed us to establish that the solar corona expands very rapidly close to the Sun (Antonucci et al. 1997a; Kohl et al. 1997; Noci et al. 1997). The first analyses of the O VI doublet lines indicated that in polar coronal holes the wind speed exceeds 100 km s^{-1} very close to the Sun (Antonucci et al. 1997a; Habbal et al. 1997; Kohl et al. 1997; Noci et al. 1997). It increases to reach 300–400 km s^{-1} at about 3 $R_\odot$ (e.g. Giordano et al. 1997; Kohl et al. 1998) and beyond 1.5 $R_\odot$ is faster in the dim coronal regions that can be identified with interplume regions (Giordano et al. 2000a; Teriaca et al. 2003).

The study of the O VI line intensity ratio has also shown that in polar coronal holes, at least above 1.8 $R_\odot$, the velocity distribution of the oxygen ions is highly anisotropic (Kohl et al. 1997, 1998; Li et al. 1998; Cranmer et al. 1999b; Antonucci et al. 2000; Giordano et al. 2000b). The rapid increase in oxygen temperature from 6×10^6 K at 1.5 $R_\odot$ to $2–3 \times 10^8$ K at 2.8 $R_\odot$ (e.g. Antonucci et al. 2000) and the broad anisotropic velocity distributions across the magnetic field in the regions of acceleration of the fast solar wind suggest that these unexpected velocity distributions are the main signature of the solar wind acceleration mechanism. This is also implied by the fact that the faster wind, that is the higher wind acceleration, observed in the interplume regions is associated with higher kinetic temperatures (Antonucci et al. 1997a). These effects have been ascribed to energy deposited in the oxygen wind component preferentially across the magnetic field, due probably to ion-cyclotron resonance heating by high frequency Alfvén waves (Kohl et al. 1998; Cranmer et al. 1999b). The results on the oxygen component of the fast solar wind have been recently reviewed by Antonucci (2006) and Kohl et al. (2006).

In this paper a detailed analysis of the dynamical properties of the fast solar wind above polar coronal holes is performed, in order to extend the measurement of the oxygen kinetic temperature and outflow velocity out to 5 $R_\odot$. Secondly we intend to investigate the O^{+5} velocity distribution beyond 3.5 $R_\odot$ in order to verify which is the extent of the coronal range where the distribution is constrained to be anisotropic and, in turn, where energy is deposited preferentially across the magnetic field, with implications for the mechanism of heating and acceleration of oxygen ions in polar coronal holes.

2. Diagnostic method

Main aim of this work is to extend the region where the outflow velocity of the oxygen component of the fast wind is inferred out to 5 $R_\odot$, in the attempt to get closer to the altitude where the asymptotic speed of 750–800 km s^{-1} is observed at about 8 $R_\odot$, according to interplanetary scintillation (IPS) observations (e.g. Grall et al. 1995).

On the basis of the Doppler dimming technique used to infer the radial outflow velocity of an expanding corona we need to

Article published by EDP Sciences and available at http://www.aanda.org or http://dx.doi.org/10.1051/0004-6361:20077083

determine the 3D-dimensional velocity distribution of the coronal absorption ions. However, only the velocity distribution of the emitting ions along the line of sight (LOS) can be directly inferred from the width of the O VI 1032 line profile; whilst the Doppler dimming technique itself, when applied to the ratio of the O VI doublet intensity, can constrain the unknown distribution along the radial direction. Therefore the O^{+5} kinetic temperature on the plane of the sky (POS) have to be accurately inferred, by taking into account all the physical and instrumental contributions to the emission of the volume element of the corona on the POS. This will be done by obtaining a best fit of the data as explained in the following.

2.1. O^{+5} kinetic temperature

The profile of the solar spectrum in the range from 1020 Å to 1045 Å, where the O VI doublet originates, is determined by the blending of intense (O VI doublet at 1031.92 and 1037.61 Å and H I 1025.72 Å) and very faint lines (such as Fe III 1035.77 Å and C II doublet at 1036.34 and 1037.02 Å). These lines are broadened by the velocity distribution of the emitting ions and atoms along the LOS.

Since UVCS observes the spectral emission integrated along the LOS, also the line broadening due to the Doppler effect produced by the outflow velocity of the emitting ions has a considerable effect. The oxygen kinetic temperature which can be inferred directly from the width of the O VI lines is overestimated with respect to the value on the POS. In order to consider this fact, the signal revealed by the detector has to be reconstructed, starting from the emission of the volume element of the corona on the POS (that is, on the axis of the coronal hole at height z, $P_{\mathrm{cor},z}$). The width of this elementary emission ($\sigma_{\mathrm{cor},z}$, from which the oxygen kinetic temperature on the POS will be inferred) is left as a free adjustable parameter in the fitting procedure of the UV lines detected with UVCS. The volume elements at any altitudes along the LOS are assumed to emit a Gaussian profile (e.g. Cranmer et al. 1999b), according to the local microscopic velocity distribution in the direction of the LOS perpendicular to z. Therefore the incident profile on the detector, P_{inc}, is the result of the integration along the LOS of Gaussian lines Doppler shifted according to the LOS component of the outflow velocity and Doppler dimmed according to the radial component of the outflow velocity of the emitting ions. Figure 1 shows an example of signal received by the observer (upper thick curve) and the contribution to it of the elementary components along the LOS (lower curves).

It is evident that although the individual components along the LOS have been assumed to have a Gaussian profile, the integrated line deviates from this function. The profile of P_{inc}, normalized to unity in the model, is used to fit the observed spectral lines: it depends only on the width of the signal emitted on the POS, $\sigma_{\mathrm{cor},z}$, once all the physical and dynamic parameters describing the line profile formation along the LOS are settled by employing coronal models consistent with the data.

In order to compute the shape of P_{inc} we account for the width, the emissivity and the Doppler shift, functions of the heliocentric distance, of each Gaussian component along the LOS. A spherical symmetry of the coronal hole, within a cone centered on the solar axis 60 degrees wide, is assumed. Having in mind the magnetic field configuration assumed in the analysis (Banaszkiewicz et al. 1998), this assumption derives from the fact that the field lines start to deviate significantly from a radial configuration beyond about 60 degrees. The integration in this region is performed from ($-z$ $tn60$) to (z $tn60$). At low heights the more significant contribution to P_{inc} is given by the emission near the polar hole axis, because of the rapid decrease in electron density and in turn in O^{+5} emissivity, with increasing heliocentric distance. For larger heliocentric altitudes, the integration path along the LOS must be larger since the electron density decreases more slowly and therefore also the emissions far from the solar axis contribute significantly to the incident profile. For all the heliocentric heights, a further increase of the integration interval involves a width variation <5%. The integration step in the analysis is 0.1 $R_\odot$.

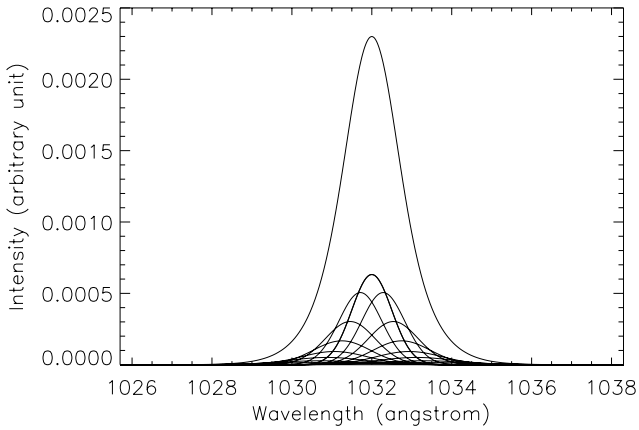

Fig. 1. Incident signal received by the observer (*upper curve*), sum of the elementary components along the LOS (*lower curves*); the thick curve represents the signal $P_{\mathrm{cor},z}$, whose width has to be derived; z = 2 $R_\odot$; the integration is performed from −3.5 $R_\odot$ to 3.5 $R_\odot$ along the LOS.

2.1.1. O VI line Doppler shift along the LOS

The Doppler shift of each component of P_{inc} is computed on the basis of a model of the outflow velocity and the magnetic configuration. The Doppler shift is determined by the component of the outflow velocity vector (whose direction is given by the magnetic field vector $\boldsymbol{B}$) parallel to the LOS, v_{LOS}, according to the formula:

$$\Delta\lambda \cong \lambda \frac{v_{\mathrm{LOS}}}{c} \sin^2 \phi, \tag{1}$$

where ϕ is the angle between the direction from the center of the Sun to the emitting volume element and the LOS (Antonucci et al. 1997b).

The magnetic model of Banaszkiewicz et al. (1998) is assumed for describing the magnetic field at solar minimum corona. The parameters that describe this model are set as: M = 1.789, Q = 1.5, K = 1.0, a_1 = 1.538.

For the first analysis of the oxygen kinetic temperature we employ a semi-empirical model to describe the outflow speed of the oxygen component of the fast solar wind; it has been derived in such a way to be compatible with the previous results by Antonucci et al. (2004) at low heliocentric distances (the initial velocity is set to 80 km s^{-1} at 1.5 $R_\odot$) and with the asymptotic outflow velocity $v_\infty \sim 750{-}800$ km s^{-1}, which is achieved certainly at ~20 $R_\odot$ (Breen et al. 1996), but probably even at ~8 $R_\odot$, according to interplanetary scintillation observations (e.g. Grall et al. 1995). The resulting outflow velocity as a function of the heliocentric distance in the coronal hole is shown in Fig. 2.

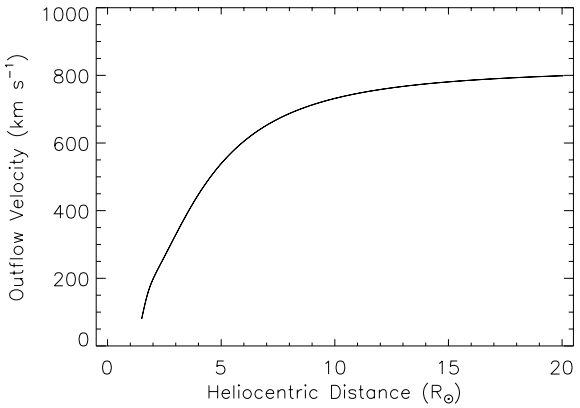

Fig. 2. Polar coronal velocity model: the wind speed is close to its asymptotic value at ~20 $R_\odot$.

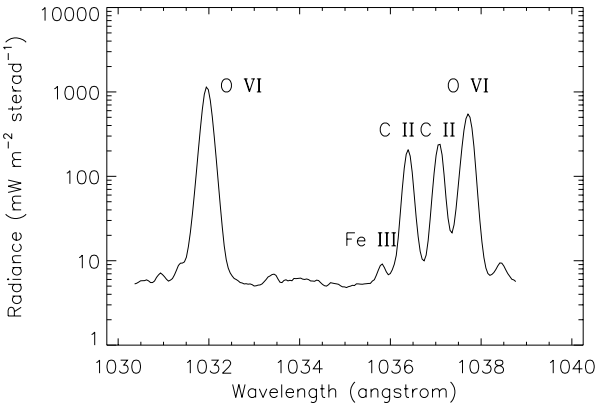

Fig. 3. Spectral region of the solar disk observed by Curdt et al. (2001) with SUMER.

As a subsequent step, after the oxygen kinetic temperature has been obtained in first approximation, we infer it again. In this second step, in order to compute the Doppler shift of each component of $P_{\rm inc}$, we employ the speed of the oxygen component of the fast solar wind, derived by applying the spectroscopic diagnostics described in Sect. 2.2. and which accounts for the oxygen kinetic temperature, instead of the model shown in Fig. 2. Throughout this iterative procedure we make us sure that the new inferred oxygen kinetic values are consistent with the previous ones, within the statistical uncertainties.

2.1.2. O VI line width along the LOS

The width of the coronal spectral line is a function of the heliocentric distance. Therefore the width of each component of $P_{\rm inc}$ varies along the LOS. In order to compute the incident profile we actually need only the variation of the O VI line width with the heliocentric distance, since the width of the signal emitted on the POS is left as a free adjustable parameter in the fitting procedure: once its value is fixed in the fitting procedure the values of the width of the other components along the LOS are constrained to vary with the employed model. In such a way, in the fitting procedure the width of each component of $P_{\rm inc}$ depends on the width $\sigma_{{\rm cor},z}$ of $P_{{\rm cor},z}$, which is an adjustable parameter and has to be derived. In first approximation the line width is assumed to be constant throughout the LOS and thus equal to $\sigma_{{\rm cor},z}$. In a subsequent step, once the O VI line widths are obtained from the analysis, the fitting procedure is iterated by taking into account that their evolution with the heliocentric distance is generally different from that previously assumed in first approximation. This iterative procedure is performed until input and output line widths converge, within the statistical uncertainties.

2.1.3. O^{+5} emissivity along the LOS

The coronal emissivity consists of a collisional and a radiative component. The collisional component, expressed in photons cm^{-3} s^{-1} sterad^{-1}, which depends only on local quantities, is given by the following formula:

$$E_{\rm coll} = \frac{1}{4\pi}\, b\, n_{\rm e}\, n_{\rm i}\, q_{\rm coll}, \tag{2}$$

where $n_{\rm e}$ is the polar coronal electron density, $n_{\rm i}$ is the number density of the O^{+5} ions, b is the branching ratio for radiative de-excitation and $q_{\rm coll}$ is the collisional excitation rate coefficient of the atomic transition (Elwert 1952; Gabriel & Jordan 1972).

In Antonucci et al. (2004) a new spectroscopic method has been developed in order to derive both the electron density and the outflow velocity from UVCS data, given the constrain of mass flux conservation in the flow tube connecting the open field corona to the heliosphere. The electron density results by Antonucci et al. (2004) are consistent with the model proposed by Guhathakurta et al. (1999). Therefore in this paper we employ this model for the polar coronal electron density.

The collisional coefficient $q_{\rm coll}$, and in turn $E_{\rm coll}$, is a function of the electron temperature, $T_{\rm e}$. This quantity has been assumed in such a way to be compatible at low heliocentric distances with the values by David et al. (1998) and at large heliocentric distances with the value of $\sim 1 \times 10^5$ K achieved at 1 AU (e.g. Schwenn 1990).

The radiative component expressed in photons cm^{-3} s^{-1} sterad^{-1} is given by the following formula:

$$E_{\rm rad} = \frac{1}{4\pi}\, b\, n_{\rm i}\, h\, \lambda_0\, B_{12} \int_\Omega \Phi(\delta\lambda) p(\varphi) {\rm d}\omega, \tag{3}$$

where B_{12} is the Einstein coefficient for absorption (e.g. Antonucci et al. 2004). In Eq. (3), $\Phi(\delta\lambda)$ is the Doppler dimming factor introduced by the dynamics of the expanding plasma

$$\Phi(\delta\lambda) = \int_0^{+\infty} I_{\rm ex}(\lambda - \delta\lambda, \boldsymbol{n})\, \Psi(\lambda - \lambda_0)\, {\rm d}\lambda, \tag{4}$$

where $\delta\lambda$ is the shift of the disk spectrum introduced by the radial expansion velocity of the coronal absorbing ions along the direction of the incident radiation, $\boldsymbol{n}$, and $I_{\rm ex}(\lambda, \boldsymbol{n})$ is the intensity of the exciting spectrum emitted from the lower atmosphere along the direction $\boldsymbol{n}$. The spectrum brightness on the solar disk assumed in the analysis is that observed by Curdt et al. (2001) with the Solar Ultraviolet Measurements of Emitted Radiation (SUMER) and shown in Fig. 3, thus we are sure to take correctly into account the effect of the optical pumping and the real continuum incident solar disk spectrum. The disk intensities are corrected to take into account the limb brightening of the transition region O VI lines by considering a non-uniform distribution over the disk that approximates the one observed with the SUMER spectrometer (A. H. Gabriel & J.-C. Vial, private communication). This aspect of the analysis is more important in the inner corona than in the extended corona.

The velocity distribution of the absorbing ions along the direction $\boldsymbol{n}$ represented by the normalized coronal absorption profile, $\Psi(\lambda, \boldsymbol{n})$, sets the assumed degree of anisotropy. In particular, if $T_{{\rm OVI},\parallel} = T_{\rm e}$ the degree of anisotropy is maximum, while if

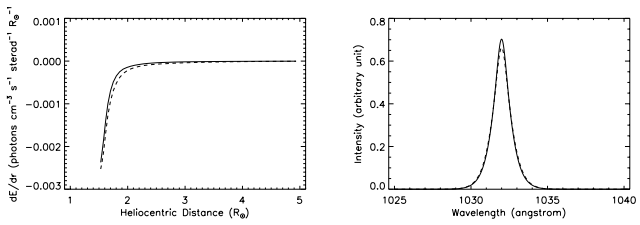

Fig. 4. Derivative of the O VI 1032 emissivity (*left panel*) and observed O VI 1032 profile at 2 $R_\odot$ (*right panel*), computed by assuming maximum anisotropy (continuous line) and isotropy (dashed line) of the oxygen ion velocity distribution.

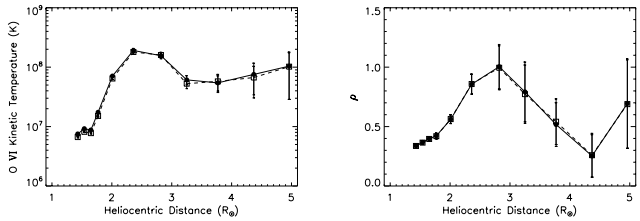

Fig. 5. O VI kinetic temperature (*left panel*) and O VI 1037−1032 line intensity ratio (*right panel*) inferred and computed by assuming isotropy (open squares joined with a dashed line) and maximum anisotropy (full dots joined with a continuous line) of the oxygen ion velocity distribution.

$T_{\mathrm{OVI},\perp} = T_{\mathrm{OVI},\parallel} = T_{\mathrm{k,OVI}}$ the ion velocity distribution is isotropic. The choice of the degree of anisotropy (either anisotropic or isotropic) of the velocity distribution is not crucial in synthesizing the observed spectral profile. The reconstruction of the line profile model to be fitted, and in turn the inference of the O VI 1032 line width and the oxygen kinetic temperature on the POS, indeed depend on how the emissivity varies with the heliocentric distance, which is not strongly depending on the degree of anisotropy of the ion velocity distribution, as shown in the left panel of Fig. 4, where the derivatives of the O VI 1032 emissivity, computed for the two extreme boundaries for the oxygen temperature anisotropy, are shown and compared. In order to clarify this point the right panel of Fig. 4 shows that the observed O VI 1032 profiles at 2 $R_\odot$, reconstructed by considering isotropy (dashed line) or maximum anisotropy (continuous line) of the oxygen ion velocity distribution, are almost coincident.

Thus, since the reconstruction does not significantly depend on the degree of anisotropy assumed in the analysis, also the O VI kinetic temperature and 1037−1032 line intensity ratio inference and computation are not noticeably affected by this assumption, as shown in Fig. 5 where we anticipate the results presented in Sect. 4.

Thus all the results presented throughout this paper are inferred by considering an isotropic velocity distribution of the oxygen ions, except for what concerns the outflow velocity of the oxygen component of the fast wind, which instead is strongly influenced by the temperature anisotropy (see Fig. 12 in Sect. 4).

2.1.4. Observed spectrum computation and fitting procedure

The profile, normalized to unity, of the signal received by the observer, P_{inc}, is evaluated by using the following formula:

$$P_{\mathrm{inc}}(\lambda) = \frac{P_{\mathrm{cor},z}(\lambda) + \sum_i P_{\mathrm{cor},i}(\lambda)}{E_{\mathrm{tot}}(P_{\mathrm{cor},z}) + \sum_i E_{\mathrm{tot}}(P_{\mathrm{cor},i})}, \tag{5}$$

where the sum is performed along the LOS. This profile depends only on the width of the component on the POS, which is a free

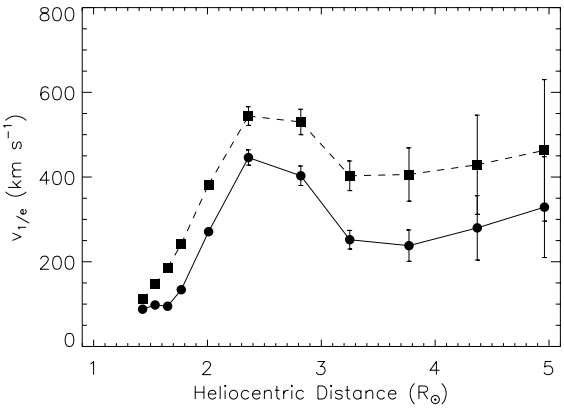

Fig. 6. Comparison of the most probable velocity of the O^{+5} ions inferred by applying the Δ correction (circles and continuous line) and without correction (squares and dashed line).

parameter in the fitting procedure. When summing the shifted components along the LOS the shape of the signal emitted on the POS ($P_{\mathrm{cor},z}$) is broadened by the Doppler effect due to the outflow velocity of the emitting ions (represented by the symbol Δ) to give the profile detected with UVCS (P_{inc}):

$$P_{\mathrm{cor},z} \xrightarrow{\Delta} P_{\mathrm{inc}}. \tag{6}$$

Therefore the local width of the coronal lines is narrower than that of observed spectra not corrected for Δ effect. In Fig. 6 we anticipate the results on the O VI kinetic temperature presented in Sect. 4. to show the effect of line broadening correction on the 1032 O VI line width σ, expressed as most probable velocity

$$v_{1/\mathrm{e}} = \sqrt{2}\frac{c}{\lambda_0}\sigma, \tag{7}$$

observed in the southern coronal hole on 1997 December 20−22 and 31.

If the Δ correction is applied, the O VI 1032 line width becomes smaller, with an average reduction of 35%. The corresponding reduction in the inferred O VI kinetic temperature is of 55%.

The correction for the additional contributions of the chromospheric radiation, recorded as stray light with UVCS, is applied by using chromospheric lines that, although non generated in corona, are detected by the instrument, such as the C III line at 977 Å, acting as stray light monitor lines (Giordano 1999). From their intensity as a function of heliocentric distance, it is possible to infer and, in turn, subtract the contribution of stray light to O VI coronal lines, by means of the width and the intensity of the O VI chromospheric lines. The stray light correction is applied on the O VI doublet. Its contribution to line width is <10%.

The response of the optical components of the instrument and the width of the spectrometer slit modify and broaden the incident profiles. This contribution is removed from the observed spectra by using the instrumental profile defined as the profile produced by a monochromatic radiation passing through the spectrometer slit with a width set at 9 μm. The observed profile is thus given by the convolution of the profile reaching the detector, the instrumental profile (P_{ins}, a Lorentzian function with $FWHM = (1.2 \pm 0.1)$ pxl; Giordano 1999) and the function that represents the slit width (S_{w}, approximated to a rectangular profile as wide as the number of the illuminated detector pixels). The instrumental correction implies a reduction of the O VI 1032 line width by ∼20%.

The continuum intensity, which is linearly dependent on wavelength, has been subtracted.

The observed profile is synthesized in the fitting procedure in this way: the signal emitted by the O^{+5} ions on the POS, $P_{\mathrm{cor},z}$, whose width is left as a free adjustable parameter, is broadened by the Doppler effect due to the outflow velocity of the emitting ions to produce the signal incident into the detector, P_{inc}. This physical effect, described by the symbol Δ (see Eq. (6)) is applied to the three lines analyzed: O VI doublet at 1031.9 and 1037.6 Å and H I at 1025.7 Å. Microscopic velocity distribution of the emitting ions and atoms in the outer corona can be very large with increasing heliocentric distance, as shown by the UVCS observations, thus the blending of wings of the O VI doublet and H I Lyβ lines cannot be neglected, in order to avoid an overestimation of the oxygen line width. Hence:

$$P_{\mathrm{inc}} = P_{\mathrm{inc,HI}} + P_{\mathrm{inc,OVI,1032}} + P_{\mathrm{inc,OVI,1037}}. \quad (8)$$

The stray light contribution to O VI doublet must be summed to the P_{inc} signal. Thus the incident signal becomes:

$$P_{\mathrm{inc}} = P_{\mathrm{inc}} + P_{\mathrm{sl}}, \quad (9)$$

where P_{sl} is the stray light contribution signal. The stray light signal, being chromospheric in origin, is indeed broadened only by the instrumental response and not by the Doppler effect due to the outflow velocity of the emitting ions, as for the coronal lines. Finally the observed profile is the convolution of the incident signal with the instrumental profile P_{ins} and with the slit width function S_{w}, summed to the background function *bckg*:

$$P_{\mathrm{obs}} = P_{\mathrm{inc}} * P_{\mathrm{ins}} * S_{\mathrm{w}} + bckg. \quad (10)$$

The reconstructed observed profile is compared with the experimental UVCS data in the χ^2 minimization. The best fit is obtained by applying the Levenberg-Marquardt least squares minimization method with the following quantities as adjustable parameters for each line of the observed spectrum: standard deviation σ of the emission on the POS, mean wavelength λ_0 of the solar profile, and the intensity of the signal integrated along the LOS. Furthermore also the slope and intercept of the background are adjustable parameters.

The width of the O VI 1032 line emission on the POS, $\sigma_{\mathrm{cor},z}$, obtained from the fitting analysis, allows us to infer the oxygen kinetic temperature $T_{\mathrm{k,OVI}}$ on the POS with the following formula:

$$T_{\mathrm{k,OVI}} = \left(\frac{\sigma_{\mathrm{cor},z}\, c}{\lambda_0}\right)^2 \frac{m_{\mathrm{O}}}{k_{\mathrm{B}}}, \quad (11)$$

where c is the speed of light, k_{B} is the Boltzmann constant, m_{O} is the oxygen mass.

2.2. O^{+5} outflow velocity

The analysis of the O VI doublet provides an accurate measurement of the O VI 1037−1032 line intensity ratio $\rho = I_{1037}/I_{1032}$, which is used as a powerful diagnostic tool to derive the speed of the oxygen component of the solar wind (Noci et al. 1987). This is because the resonantly scattered components of the O VI doublet are differently affected by the Doppler dimming, due to pumping effect of nearby lines and increasing with the outflow velocity of the corona (see Fig. 3).

Therefore, the speed of the expansion of the coronal plasma above polar holes is derived by comparing the expected O VI line intensity ratio computed by integrating along the LOS the O^{+5} emissivity, inferred on the basis of models of polar coronal electron density and temperature compatible with the observations (see Sect. 2.1.3.), with the experimental ratio derived from the data. In first approximation the semi-empirical outflow velocity model, derived on the basis of a comparison of the theoretical emissivity ratio with the observed intensity ratio (Antonucci et al. 2004) and shown in Fig. 2, has been used to derive the Doppler dimming factor and in turn the oxygen emissivity at any location along the LOS. Through a subsequent approximation stage, by employing the inferred velocity results to re-computed the O^{+5} emissivity along the LOS and in turn, by means of integration, the expected O VI doublet intensity ratio, an accurate measurement of the outflow velocity of the oxygen component of the fast solar wind on the POS is approached. This iteration is performed until input and output outflow speeds converge, within the statistical uncertainties.

The Doppler dimming is very sensitive to the intensity of the exciting spectrum emitted from the lower atmosphere. In the analysis both a quiet-Sun and a coronal hole disk spectrum have been considered (Curdt et al. 2001). Negligible differences have been found in the results of the wind velocity. Hence the variation of the solar disk brightness along the LOS negligibly affects the O VI doublet intensity ratio used to infer the outflow speed of the oxygen ions.

Differently from the line width (see Sect. 2.1.3. and Figs. 4 and 5), the Doppler dimming, and in turn the expected theoretical ratio and the inferred outflow speed of the fast solar wind, are strongly dependent also on the anisotropy degree of the oxygen ion velocity distribution. The component of the oxygen temperature perpendicular to the magnetic field lines is derived from the kinetic temperature inferred from the observations: since $T_{\mathrm{k,OVI}}$ is the oxygen kinetic temperature on the POS (see Sect. 2) and the magnetic field vector is approximately parallel to the radial direction at any altitudes on the polar axis, we can reliably set $T_{\mathrm{OVI},\perp} \cong T_{\mathrm{k,OVI}}$. The unknown component of the oxygen temperature along the magnetic field lines can assume a value between the two extreme boundaries represented by the electron temperature T_{e} (maximum anisotropy) and the perpendicular component of the oxygen temperature $T_{\mathrm{OVI},\perp}$ (isotropy).

Figure 7 shows the theoretical ratio of the intensity of the O VI lines as a function of the local outflow velocity (continuous line), compared with the observed ratio (horizontal line). The dashed lines indicate the values of the outflow velocity of the expanding corona, compatible with the observation.

From the comparison of the expected O VI line intensity ratio with the experimental value two solutions are generally found for large heliocentric distances. In order to maintain a positive acceleration for the fast wind, the outflow velocity that assures that $v(r_{i+1}) > v(r_i)$ is chosen.

3. Observations

The analysis is applied to the observations performed with the Ultraviolet Coronagraph Spectrometer (UVCS), from 1996 November to 1997 December during the minimum of solar cycle 23. The regions scanned by the coronagraph are coronal holes present either at the North or South pole between 1.4 $R_\odot$ and 5 $R_\odot$, depending on the data set. In Table 1 the date and region of the observations are shown.

For each observation, the slit was oriented perpendicular to the radial direction. The O VI lines were detected with spectral resolution increasing with height from a minimum value of 0.30 Å to a maximum value of 0.60 Å, in order to improve the statistics. For the same reason the duration of the observation at

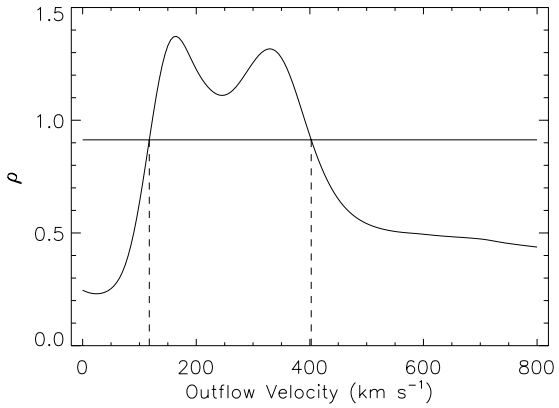

Fig. 7. Comparison between the O VI 1037−1032 line intensity ratio at 3.1 $R_\odot$ computed for a parallel component of the oxygen ion $T_{\|,\min} = T_e(r)$ (continuous curve, maximum anisotropy) with the observed one (horizontal line); the two outflow velocities compatible with the experimental value are shown (dashed lines).

Table 1. Observations performed with UVCS.

Date	*Height ($R_\odot$)*	*Pole*
November 10, 1996	3.0	North
January 9–15, 1997	3.1	North
April 14–20, 1997	3.1–4.2	South
June 7–8, 1997	2.9–3.1	North
October 18–19, 1997	1.4–3.8	North
December 20–22 31, 1997	1.4–5.0	South

any given position was chosen to increase with height. The total exposure times range from 5400 s at 1.4 $R_\odot$ to 32 000 s at 5 $R_\odot$. For a better statistics, spectra acquired on successive days at the same heliocentric distance have been summed. The slit width is narrower for lower heliocentric distances (50−100 μm) than for larger heliocentric distances (150−300 μm).

4. Results

The main novelty of the paper is the extension of the measurement of the oxygen kinetic temperature above 3.5 $R_\odot$. The coronal emission is very weak at these altitudes thus it becomes harder and harder to obtain a good fit of the data with increasing heliocentric distance. Therefore a powerful fitting tool, based on a careful synthesis of spectral line profiles, is required. In Fig. 8 all the exposures and the fits performed to UVCS data above 3.5 $R_\odot$ are shown.

For all the exposures the slit width is set to 300 μm and the spectral resolution is equal to 0.60 Å. An accurate fit of the line wings and peak is achieved. The stray light contribution is detectable from the change in the fit profile shape above 4 $R_\odot$: the stray light signal, being chromospheric in origin, is broadened only by the instrumental response and not by the Doppler effect due to the outflow velocity of the emitting ions as for the coronal lines. Figure 8 shows the linearly dependence of the background on wavelength and the blending of wings of the O VI doublet and H I Lyβ. The statistics of the data is considered sufficient as shown by the statistical errors reported in the figure. Although the statistics is getting worse with increasing heliocentric distance, these exposures and the relative fit curves show that it is possible to observe at altitudes larger than 3.5 $R_\odot$ in corona.

The O VI 1032 coronal intensity as a function of the heliocentric distance is shown in Fig. 9.

The coronal intensity of the O VI 1032 line is larger than the chromospheric stray light signal considered in the analysis for any heliocentric distance. At 5 $R_\odot$ the coronal intensity of the O VI 1032 line, inferred from the observation performed on December 31, 1997 at the South pole, is 1.24×10^5 photons cm^{-2} s^{-1} sterad^{-1} ± 30%, whilst the intensity of the stray light contribution is about 0.27×10^5 photons cm^{-2} s^{-1} sterad^{-1}. Hence up to 5 $R_\odot$ the intensity of the O VI line emitted by the corona is at least five times larger than the one emitted by the chromosphere. This ensures that the analysis is always performed on coronal signals.

The observed intensity in the polar holes varies depending on the observation date. It is possible to show that there is a systematic effect due to the inclination of the solar axis. Since the orbit of the Earth lies on a different plan from that of the solar equator, the solar axis appears to vary continually its inclination in the course of the year. It appears vertical only on December 7 and June 7, whilst its inclination reaches the maximum value on March 7 and September 7. Therefore when the Solar axis is approximately vertical with respect to the ecliptic (in December and June: green and dark blue circles in Fig. 9, respectively) the observed intensity is smaller than that observed in the other periods of the year when the quiet sun region adjacent to the coronal hole, where the electron density is larger, also contributes to the emission integrated along the LOS in addition to the coronal hole signal. Green and dark blue circles correspond hence to the actual coronal hole observations.

The oxygen kinetic temperatures on the POS as a function of the heliocentric distance, inferred by accounting for the effect of line broadening due to the Doppler effect produced by the coronal expansion along the LOS direction, are shown in Fig. 10. The results indicated by the solid thick line are the averages over the data sample. They are compared with the results by Antonucci et al. (2004) (black full squares) inferred without correction for this effect and with the result by Cranmer et al. (1999b) which is a best-fit function to the experimental data valid between 1.5 $R_\odot$ and 3.5 $R_\odot$.

The oxygen kinetic temperature remains almost constant from 1.4 $R_\odot$ to 1.7 $R_\odot$ at the average value of $\sim 7.1 \times 10^6$ K. Beyond 1.7 $R_\odot$ the oxygen temperature sharp increases to reach a maximum value of 1.5×10^8 K at 2.9 $R_\odot$. Further out the curve representing the averaged values is flattening although there are fluctuations with the increasing heliocentric distance, probably related to different physical conditions of the solar corona in the periods analyzed. Particularly the oxygen temperature measurements above polar holes when the solar axis is closer to the POS are indicated by green and dark blue circles in Fig. 10. The values of the O^{+5} kinetic temperature derived by taking into account the line broadening due to Doppler shifts produced by the expansion of the corona are of the same order of those obtained from the previous analysis in Antonucci et al. (2004), but generally 55% smaller. Out to 2.9 $R_\odot$ the results by Cranmer et al. (1999b) are consistent with the present ones. For larger heliocentric distances the best-fit function by Cranmer et al. (1999b) still increases, contrary to the values inferred in this analysis, although the fluctuation of the oxygen kinetic temperature values is large.

The O VI 1037−1032 line intensity ratio as a function of the heliocentric distance is shown in Fig. 11. The results indicated by the solid thick line are the averages over the data sample.

The experimental line intensity ratio increases from 0.4 at 1.4 $R_\odot$ to 1.0 at 2.8 $R_\odot$. Beyond this height, it decreases to reach the value of 0.5 at 4.5 $R_\odot$. According to the behavior of the averaged curve, beyond 4.5 $R_\odot$ the O VI line intensity ratio has

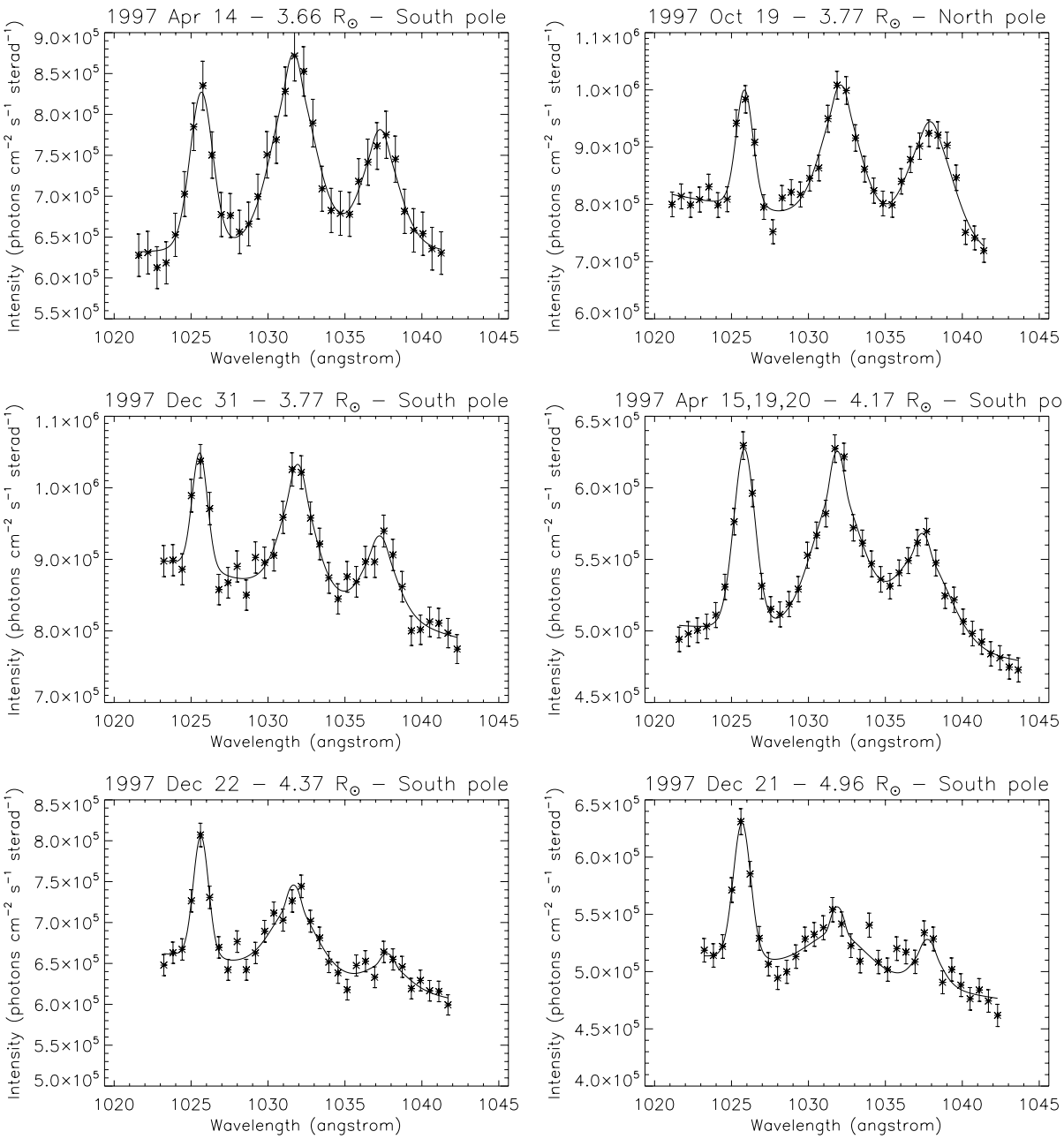

Fig. 8. Observed UVCS spectra with the fit curves (thick and continuous line).

been extrapolated to the value of 0.5, compatible with the experimental data at 4.96 $R_\odot$ equal to 0.665, since the error bars are very large (relative error of 54%). Moreover this extrapolation is consistent with the theoretical intensity ratio inferred by assuming the electron density by Guhathakurta et al. (1999), the intensity of the exciting spectrum emitted from the lower atmosphere given by Curdt et al. (2001) and the O VI kinetic temperature derived in the present analysis. However at 5 $R_\odot$ the emission process is still not collisionally dominated, since the radiative component of the emissivity is only ∼4 times smaller than the collisional one and thus the outflow velocity can be still inferred by using the diagnostics described in Sect. 2 below.

The Doppler dimming analysis applied to derive the speed of the oxygen component of the fast solar wind is performed by using the averaged values of the O VI kinetic temperature and line intensity ratio shown in Figs. 10 and 11 (thick continuous lines). The outflow velocity, derived by assuming maximum anisotropy and isotropy in the oxygen ion velocity distribution (full and open red dots, respectively) is plotted in Fig. 12. In the top panel it is compared with the results by Antonucci et al. (2004) (black dots), whilst in the bottom one with the curves by Cranmer et al. (1999b) (dotted and dashed lines).

The outflow velocity of the fast solar wind increases monotonically outward to reach 550 km s^{-1} or 760 km s^{-1} at 5 $R_\odot$ in the case of maximum anisotropy and isotropy of the oxygen ion velocity distribution, respectively. Since the oxygen temperature parallel to the radial direction is not directly measured it is possible to derive the outflow velocity of the fast solar wind only in a relative wide acceptance region, by assuming the two extreme boundaries compatible with the data of the anisotropy in the oxygen ion velocity distribution. The region within the two curves inferred in such a way defines the accuracy in deriving

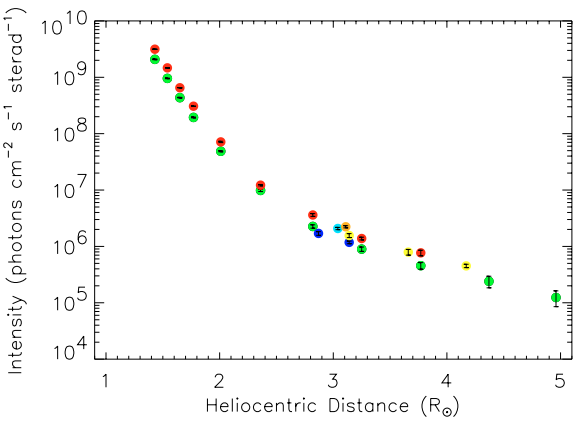

Fig. 9. O VI1032 coronal intensity as a function of the heliocentric distance: green circles correspond to the observation performed on 1997 December; red circles on 1997 October; blue circles on 1996 November; dark blue circles on 1997 June; orange circles on 1997 January; yellow circles on 1997 April.

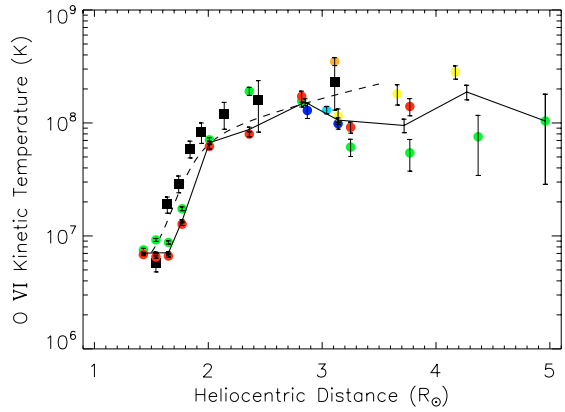

Fig. 10. O VI kinetic temperature as a function of the heliocentric distance: green circles correspond to the observation performed on 1997 December; red circles on 1997 October; blue circles on 1996 November; dark blue circles on 1997 June; orange circles on 1997 January; yellow circles on 1997 April; the solid thick line represents the averaged values; the results not accounting for the line broadening caused by the Doppler effect due to the expanding corona are the black full squares for the 1996 May observation (Antonucci et al. 2004); the dashed line represents the results by Cranmer et al. (1999b).

the velocity of the oxygen component of the fast wind and the region where all the other possible solutions consistent with the data are falling.

In the case of isotropy of the oxygen ion velocity distribution the values of the velocities of the fast wind are generally smaller than those inferred in the previous analyses by Antonucci et al. (2004) and Cranmer et al. (1999b). In the case of maximum anisotropy of the oxygen ion velocity distribution the behavior of the speed of the fast coronal wind as a function of the heliocentric distance is quite different, particularly from 1.8 $R_\odot$ to 2.8 $R_\odot$, where the present results are significantly lower than previous ones. The differences between the present results and those inferred by Antonucci et al. (2004) might be ascribed to the fact that the latter ones have been obtained by comparing the observed O VI line intensity ratio with the expected O VI 1037−1032 ratio of the emissivity on the POS.

Figure 12 shows that for an isotropic velocity distribution of the oxygen ions in the altitude region from 2 $R_\odot$ to 3.7 $R_\odot$, there is no physical solution for the outflow velocity of the expanding

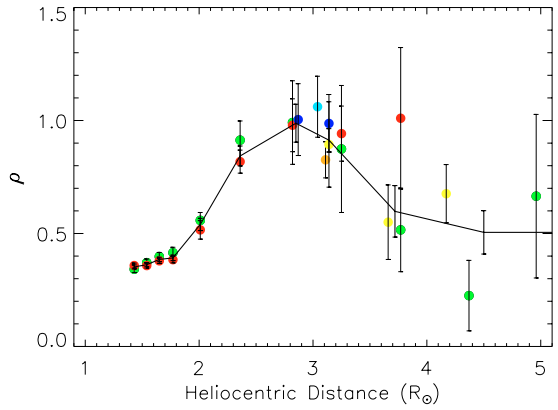

Fig. 11. O VI 1037–1032 line intensity ratio ρ derived from the spectra observed with UVCS in the days reported in the Table 1: green circles correspond to the observation performed on 1997 December; red circles on 1997 October; blue circles on 1996 November; dark blue circles on 1997 June; orange circles on 1997 January; yellow circles on 1997 April; the thick continuous line represents the averaged values.

plasma; that is the observed O VI line intensity ratio never intercepts the expected curve.

5. Discussion

In this paper we have extended out to 5 $R_\odot$ the measurement of the expansion speed of the oxygen component of the fast wind with the aim to get closer to the region where the asymptotic value of 750−800 km s^{-1} is achieved, as observed at about 8 $R_\odot$ with scintillation techniques. At the same time we have extended the investigation of the degree of anisotropy of the O^{+5} velocity distribution out to the same coronal altitude. The latter quantity is of crucial importance being related to the mechanism of energy deposition in the region of acceleration of the solar wind in the outer corona. Since at the poles the magnetic field lines run approximately along the radial direction, an excess of width of the velocity distribution along the LOS has been suggested to indicate preferential acceleration of the oxygen ions across the coronal magnetic field, due very likely to ion-cyclotron resonance scattering by high frequency Alfvén waves (Kohl et al. 1998; Cranmer et al. 1999b).

It is well known from the previous literature that the oxygen velocity distribution is constrained to deviate from isotropy beyond 2 $R_\odot$ (e.g. Kohl et al. 1997; Dodero et al. 1998; Kohl et al. 1998, 1999; Cranmer et al. 1999a,b; Antonucci et al. 2000; Giordano et al. 2000b; Antonucci et al. 2004). However the previous analyses were performed only out to 3.5 $R_\odot$ and therefore it was not possible on their bases to limit the coronal region where the energy deposition, by means of ion-wave processes, and the consequent acceleration of the oxygen ions occur. Hence the present analysis allows us to investigate the degree of anisotropy of the oxygen ion velocity distribution beyond 3.5 $R_\odot$. A further aim of this paper, in which the contribution to the line width of the Doppler effect due to the expanding plasma has been assessed, resides on the necessity to check and possibly confirm the important results achieved by the UVCS team on the oxygen temperature anisotropy, recently questioned by considering the effect of the LOS integration on O VI line broadening, with consequent implications on heating and accelerating process of O^{+5} in polar coronal holes (e.g. Raouafi & Solanki 2004, 2006).

The results of the analysis show that it is impossible to interpret the Doppler dimmed emission of the outer corona by

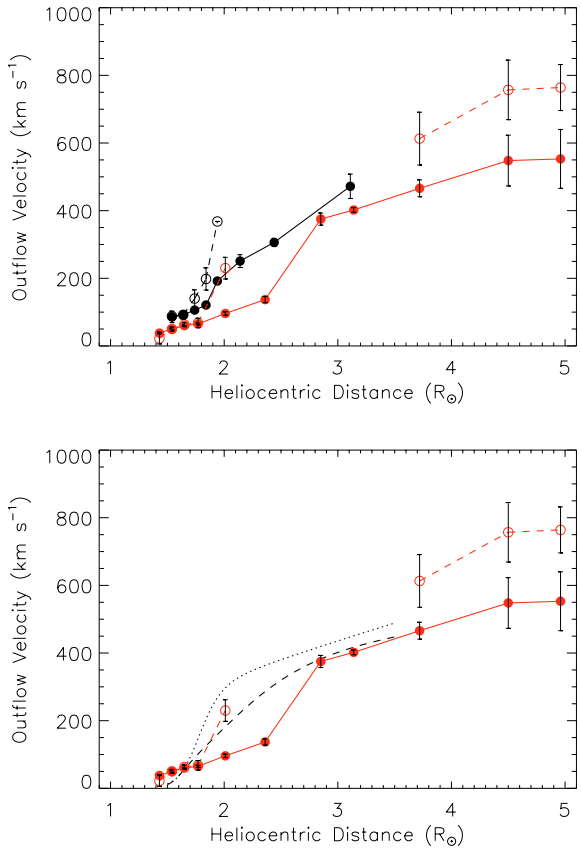

Fig. 12. Oxygen outflow velocity as a function of the heliocentric distance (red dots); full signs are for the results obtained by considering the maximum anisotropy of the oxygen ion velocity distribution, whilst open signs are for the results obtained, when possible, by using the isotropic configuration; *top panel*: black dots are for the 1996 May observation (results by Antonucci et al. 2004); *bottom panel*: the dashed and dotted lines represent the results by Cranmer et al. (1999b), in the case of maximum anisotropy and isotropy respectively.

assuming an isotropic velocity distribution of the oxygen ions beyond 2 $R_\odot$ and out to 3.7 $R_\odot$, thus confirming the classical UVCS results, although the Doppler effect due to the coronal expansion affects the line width (oxygen kinetic temperatures ~55% smaller than in previous analyses are derived). The results indicate also that the energy deposition process is certainly acting in a layer of almost 2 $R_\odot$, from 2 $R_\odot$ to 3.7 $R_\odot$, thus identifying a coronal region where the energy is necessarily deposited preferentially across the magnetic field lines. This is the region where Alfvén waves interact in the solar corona with particles of charge to mass ratio equal to 0.3. Furtherout, above 3.7 $R_\odot$, anisotropy of the oxygen ion velocity distribution can still exist but not necessarily.

The extension of the measurement of the kinetic temperature and outflow velocity of the O^{+5} ions out to 5 $R_\odot$ allows us to address the question whether the speed of the fast solar wind is indeed reaching the asymptotic value of 750−800 km s^{-1} observed at about 8 $R_\odot$ with scintillation techniques. The outflow velocity of the oxygen component of the fast wind, obtained by considering the maximum anisotropy in the ion velocity distribution, reaches a value of 550 km s^{-1} at 4.5 $R_\odot$, far from the asymptotic speed. In this case, an almost steady state regime is established beyond 4.5 $R_\odot$, since the outflow velocity at 5 $R_\odot$ remains at 550 km s^{-1}. Therefore, by considering the maximum anisotropy in the oxygen ion velocity distribution, the speed of the expanding corona does not appear to be consistent with the interplanetary scintillation observations (e.g. Grall et al. 1995). The alternative possible solution is the existence as an isotropic distribution of the oxygen ions beyond 3.7 $R_\odot$. The corresponding outflow velocity in this case is much larger. An isotropic distribution is reached if the energy deposited across the magnetic field in the altitude region from 2 $R_\odot$ to 3.7 $R_\odot$ has been transferred to the radial direction beyond 3.7 $R_\odot$ and the energy deposition across the field is not any longer as efficient as in the 2 $R_\odot$ to 3.7 $R_\odot$ region. In this case the speed of the oxygen component of the fast solar wind reaches 760 km s^{-1}, a value very close to the asymptotic speed. Therefore by considering isotropy of the ions beyond 3.7 $R_\odot$, it is possible to assert that the asymptotic speed observed at about 8 $R_\odot$ is achieved. However in this case it is necessary to propose a physical scenario for the variation of the anisotropy ratio with increasing height, since the velocity distribution of the ions is constrained to be anisotropic from 2 $R_\odot$ to 3.7 $R_\odot$. The most plausible evolution of the degree of anisotropy throughout the corona will be assessed in a next paper.

Acknowledgements. This work was supported by the Italian Space Agency (ASI) grants (I/035/05/0). Daniele Telloni is a PhD student with a fellowship of the National Institute for Astrophysics (INAF).

References

Antonucci, E. 2006, Space Sci. Rev., 124, 35
Antonucci, E., Noci, G., Kohl, J. L., et al. 1997a, ASP Conf. Ser., 118, 273
Antonucci, E., Kohl, J. L., Noci, G., et al. 1997b, ApJ, 490, L183
Antonucci, E., Dodero, M. A., & Giordano, S. 2000, Sol. Phys., 197, 115
Antonucci, E., Dodero, M. A., Giordano, S., Krishnakumar, V., & Noci, G. 2004, A&A, 416, 749
Banaszkiewicz, M., Axford, W. I., & McKenzie, J. F. 1998, A&A, 337, 940
Breen, A. R., Coles, W. A., Grall, R. R., et al. 1996, Ann. Geophys., 14, 1235
Cranmer, S. R., Field, G. B., & Kohl, J. L. 1999a, ApJ, 518, 937
Cranmer, S. R., Kohl, J. L., Noci, G., et al. 1999b, ApJ, 511, 481
Curdt, W., Brekke, P., Feldman, U., et al. 2001, A&A, 375, 591
David, C., Gabriel, A. H., Bely-Dubau, F., et al. 1998, A&A, 336, L90
Dodero, M. A., Antonucci, E., Giordano, S., & Martin, R. 1998, Sol. Phys., 183, 77
Elwert, G. 1952, Z. Naturforsch., 7a, 432
Gabriel, A. H., & Jordan, C. 1972, Case Studies in Atomic Collision Physics, Vol. 2, ed. McDaniel, & McDowell (North Holland)
Giordano, S. 1999, Ph.D. Thesis, Università degli Studi di Torino
Giordano, S., Antonucci, E., Benna, C., et al. 1997, in 31st ESLAB Symposium, Correlated Phenomena at the Sun, in Heliosphere and in Geospace, ESA SP-415, 327
Giordano, S., Antonucci, E., Noci, G., Romoli, M., & Kohl, J. L. 2000a, ApJ, 531, L79
Giordano, S., Antonucci, E., & Dodero, M. A. 2000b, Adv. Space Res., 25, 1927
Grall, R. R., Coles, W. A., & Klinglesmith, M. T. 1995, in Observations of the solar wind speed near the sun, California Univ., International Solar Wind 8 Conference, 61
Guhathakurta, M., Fludra, A., Gibson, S. E., Biesecker, D., & Fisher, R. 1999, JGR, 104(A5), 9801
Habbal, S. R., Woo, R., Fineschi, S., et al. 1997, ApJ, 489, L103
Kohl, J. L., Esser, R., Gardner, L. D., et al. 1995, Sol. Phys., 162, 313
Kohl, J. L., Noci, G., Antonucci, E., et al. 1997, Sol. Phys., 175, 613
Kohl, J. L., Noci, G., Antonucci, E., et al. 1998, ApJ, 501, L127
Kohl, J. L., Fineschi, S., Esser, R., et al. 1999, SSRv, 87, 233
Kohl, J. L., Noci, G., Cranmer, S. R., & Raymond, J. C. 2006, A&ARv, 13, 31
Li, X., Habbal, S. R., Kohl, J. L., & Noci, G. 1998, ApJ, 501, L133
Noci, G., Kohl, J. L., & Withbroe, G. L. 1987, ApJ, 315, 706
Noci, G., Kohl, J. L., Antonucci, E., et al. 1997, Adv. Space Res., 20, 2219
Raouafi, N. E., & Solanki, S. K. 2004, A&A, 427, 725
Raouafi, N. E., & Solanki, S. K. 2006, A&A, 445, 735
Schwenn, R. 1990, in Physics of the Inner Heliosphere, ed. R. Schwenn, & E. K. Marsch (Springer Verlag), 1, 99
Teriaca, L., Poletto, G., Romoli, M., & Biesecker, D. A. 2003, Mem. S.A.It., 74, 713